analytical chemistry

pubs.acs.org/ac Article

Antibody-Free Determinations of Low-Mass, Soluble Oligomers of $A\beta_{42}$ and $A\beta_{40}$ by Planar Bilayer Lipid Membrane-Based Electrochemical Biosensor

Yuemei Duan,[‡] Jia Chen,[‡] Yan Jin, Qiuyun Tu, Shuhui Wang, and Juan Xiang*

Cite This: *Anal. Chem.* 2021, 93, 3611−3617 Read Online

ACCESS | Metrics & More | Article Recommendations | Supporting Information

ABSTRACT: Alzheimer's disease (AD) is the most common neurodegenerative disease among the elderly. Abnormal aggregates of both β-amyloid peptide ($A\beta$) subtypes, $A\beta_{42}$ and $A\beta_{40}$, are the typical neuropathology hallmarks of AD. However, because of the lack of specific recognition elements such as an antibody and aptamer, it is difficult to differentiate and determine the oligomers of $A\beta_{42}$ and $A\beta_{40}$ in clinic. In this paper, we developed a planar bilayer lipid membrane (BLM)-based electrochemical biosensor. According to the dynamic differences on oligomer-induced BLM damage, both low-mass, soluble oligomers of $A\beta_{42}$ and $A\beta_{40}$ (L-$A\beta_{42}$O and L-$A\beta_{40}$O) were measured in turn by electrochemical impedance spectroscopy. The BLM was supported by a porous 11-mercaptoundecanoic acid layer on a gold electrode, which amplified the impedance signal corresponding to the membrane damage and improved the detection sensitivity. The weakly charged surface of the BLM ensured the low non-specific adsorption of coexisting proteins in cerebrospinal fluid (CSF). Using the electrochemical biosensor, L-$A\beta_{42}$O was determined within 20 min, with a linear range from 5 to 500 pM and a detection limit of 3 pM. Meanwhile, L-$A\beta_{40}$O was determined within 60 min, with a linear range from 60 pM to 6.0 nM and a detection limit of 26 pM. The recoveries in oligomer-spiked artificial CSF and human CSF samples confirmed the accuracy and applicability of this proposed method in clinic. This work provides an antibody-free, highly selective, and sensitive method for simultaneous detections of L-$A\beta_{42}$O and L-$A\beta_{40}$O in real CSF samples, which is significant for the early diagnosis and prognosis of AD.

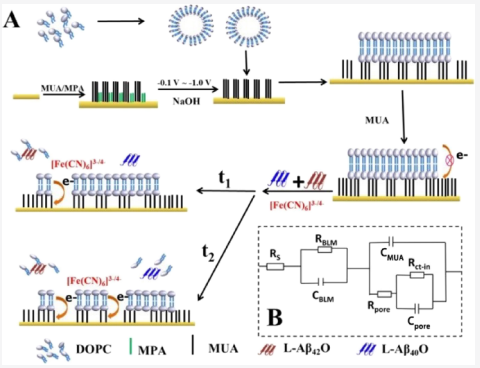

Alzheimer's disease (AD) is a neurodegenerative disease characterized by deposits of senile plaques in disease-afflicted brains. The major components of senile plaques are aggregates of an amyloid β peptide ($A\beta$) such as oligomers and fibrils.[1] Growing evidence suggests that AD is precipitated by the progressive cerebral accumulation of low-mass, soluble oligomers (L-$A\beta$O).[2,3] Therefore, L-$A\beta$O has been identified as direct agents for AD[4] and reliable molecular biomarkers for detection and diagnosis of AD.[5] $A\beta$ contains 39−43 amino acid residues, the major subtypes of which are $A\beta_{40}$ and $A\beta_{42}$.[6] Due to the structural differences, both $A\beta$ forms display distinct biophysical and clinical behaviors after aggregation.[7] The severity of cognitive deficits in AD correlates strongly with the relative levels of low-mass, soluble oligomers of $A\beta_{42}$ and $A\beta_{40}$ (L-$A\beta_{42}$O and L-$A\beta_{40}$O).[8] Therefore, accurate and specific determination of L-$A\beta_{42}$O and L-$A\beta_{40}$O is significant for a better understanding of $A\beta$-associated AD pathology and the development of early diagnosis as well as therapeutic drugs for AD.

In recent years, based on the usage of specific recognition elements, many methods such as enzyme-linked immunosorbent assay (ELISA),[9,10] fluorescence detection,[11] and electrochemical sensor[12] have been developed for the detections of $A\beta$ monomers and oligomers. The mostly used recognition elements include antibodies,[13] aptamers,[14] oligomer-specific peptides,[15] etc. When antibodies are adopted as recognition elements, due to the aggregation of $A\beta$ on its hydrophobic segment, only the hydrophilic segment is appropriate for antibody capture.[13] Since $A\beta_{40}$ and $A\beta_{42}$ have the same hydrophilic segment, these recognition elements are ineffective for the selective determination of $A\beta_{40}$ and $A\beta_{42}$ oligomers.[16] Aptamer is another kind of stable but inexpensive recognition element. Most of reported DNA aptamers target β-sheet by forming G-quadruplex structures. Note that β-sheet is a common secondary structure in aggregates of $A\beta$ and many other proteins such as α-synuclein; it results in the poor selectivity of aptamer on the detections of $A\beta_{40}$ and $A\beta_{42}$ oligomers and serious interference from coexisting α-synuclein.[14,17] Oligomer-specific peptides have good specificity

Received: December 16, 2020
Accepted: February 8, 2021
Published: February 11, 2021

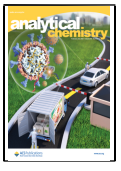

https://dx.doi.org/10.1021/acs.analchem.0c05281
Anal. Chem. 2021, 93, 3611−3617

as recognition elements to distinguish different types of Aβ oligomers. However, due to the poor sensitivity, related sensors need to amplify electrochemical signals by labeling peptide substrates and redox media, which is complicated to prepare and has a limited detection range.[18,19] Due to the limitations of present specific recognition elements, a new strategy is needed for the determination of L-Aβ_{42}O and L-Aβ_{40}O.

Compared to Aβ_{40}, Aβ_{42} has two more hydrophobic amino acids at the C-terminal, which belong to the transmembrane part of amyloid-β precursor protein. It causes Aβ_{42} to have a higher tendency to form β-sheet in the central hydrophobic nucleus (residues 17−21) and C-terminal (residues 30−42) than Aβ_{40}. Aβ_{42} oligomers have more β-folding structures (79% β-sheet) than Aβ_{40} oligomers (57% β-sheet).[20] In vitro studies further show that both oligomers can associate with lipid bilayers and cause leakage of model membranes, while L-Aβ_{42}O displays stronger affinity and faster binding kinetics than L-Aβ_{40}O in the membrane damage process.[21,22] In this paper, according to the dynamic differences on oligomer-induced membrane damage, we constructed an electrochemical biosensor by covering the planar bilayer lipid membrane (BLM) on a porous 11-mercaptoundecanoic acid (MUA)-modified Au electrode to achieve the selective determinations of L-Aβ_{42}O and L-Aβ_{40}O by electrochemical impedance spectroscopy (EIS). Compared to the compact MUA layer, the porous MUA layer on the Au electrode amplified the impedance signal changes corresponding to the membrane damage and improved the detection sensitivity. During the incubation with mixed oligomers, the sensor determined L-Aβ_{42}O and L-Aβ_{40}O in 20 and 60 min, respectively. Using this sensor, we achieved good recoveries in both oligomer-spiked artificial cerebrospinal fluid (ACSF) and human cerebrospinal fluid (CSF) samples, confirming the accuracy and applicability of this method, which is of great significance for AD detection, early screening, and diagnosis.

EXPERIMENTAL SECTION

Material and Reagents. NaCl, NaOH, KCl, $MgCl_2$, $CaCl_2$, NaH_2PO_4, $Na_2HPO_4{\cdot}7H_2O$, *N*-2-hydroxyethylpiperazine-*N*′-2-ethanesulfonic acid (HEPES), mercaptopropionic acid (MPA), MUA, 1,2-dioleoyl-*sn*-glycero-3-phosphocholine (DOPC), 3,3′-dioctadecyloxacarbocyanine perchlorate (DiO), cysteine, mercaptoethylamine, glucose, hexafluoroisopropanol (HFIP), ethylenediaminetetraacetic acid disodium salt (Na_2EDTA), and insulin were purchased from Sigma-Aldrich (Shanghai, China). $Na_4[Fe(CN)_6]$, $Na_3[Fe(CN)_6]$, H_2SO_4, and ethanol (C_2H_5OH) were purchased from Aladdin (Shanghai, China). Lyophilized Aβ_{40} and Aβ_{42} peptides were purchased from Hangzhou Dangang Biotechnology Company (Hangzhou, China). ACSF was prepared with 1 mM MgCl, 1 mM $CaCl_2$, 5 mM HEPES, 10 mM glucose, 20 mM KCl, and 140 mM NaCl. Deionized water (18.2 MΩ cm) was used in all experiments.

Apparatus and Measurements. Cyclic voltammetry (CV) and linear scanning voltammetry (LSV) were conducted on a CHI832b electrochemical workstation (Shanghai Chenhua Instrument Co., Ltd., China). EIS was conducted with a three-electrode system on a Gamry Reference 600 electrochemical workstation (Gamry Instruments Co., Ltd., Warminster, PA, USA). A BLM-modified Au electrode was used as the working electrode, and a platinum wire and a Ag/AgCl electrode were used as the counter and reference electrodes, respectively. All of the potentials in this work were with respect to the Ag/AgCl electrode. For the determination of L-Aβ_{42}O or L-Aβ_{40}O, all EIS measurements were recorded in the mixture of analyte with a 5 mM $[Fe(CN)_6]^{3-/4-}$ redox pair (1:1 molar ratio) and 0.1 M NaCl. The frequency range in the EIS measurements was from 0.1 MHz to 0.1 Hz using an AC potential of 10 mV, superimposed on a DC potential of 0.225 V. The obtained impedance data were fitted by Gamry Echem Analyst software (Gamry Instruments Co., Ltd., Warminster, PA, USA). All error bars in this paper represented the standard deviation of three parallel experiments.

Size-exclusion chromatography (SEC) measurements were conducted with high-performance liquid chromatography (HPLC) (Shimadzu LC-20 AD, Japan) equipped with a UV−vis detector (Shimadzu SPD-20A, Japan). A BioSep-SEC-s2000 column (300 mm × 7.8 mm, Phenomenex Inc.) was used. The liquid phase was 10 mM PBS (pH 7.4, 100 mM Na_2SO_4), and the flow rate was 1.0 mL/min. The retention time was calibrated with four standards (blue dextran (2000 kDa), bovine serum albumin (68 kDa), myoglobin (16.7 kDa), and vitamin B_{12} (1.3 kDa)) at 25 mg/mL. The volume of the injected sample solution was 10 μL. The elution of all species was detected with an absorbance at 220 nm.

Preparation of Phospholipid Vesicles. The phospholipid vesicles were prepared following Yamaguchi et al.'s work.[23] Briefly, 50 μL of 3 mg/mL DOPC solution (containing 5 mM DiO) was dried for 12 h in a Mikrouna Ipure glovebox (Mikrouna Co., Ltd., Shanghai, China) in which the attainable O_2 concentration was below 1 ppm. Then, 600 μL of PBS buffer (10 mM, pH 7.4) was added and sonicated at 40 Hz for 30 min to form stable and uniform phospholipid vesicles. The DOPC vesicles were characterized by a fluorescent image of DiO and dynamic light scattering, displaying an average diameter of ∼1 μm (Figure S1 in the Supporting Information). The obtained vesicle solution was stored at 4 °C for no more than 2 weeks.

Preparation of BLM-Based Electrochemical Biosensor. The porous MUA layer was fabricated following our previous work.[24] Briefly, a bare Au electrode of 2 mm in diameter was dipped into a mixed MPA (1 mM)/MUA (4 mM) ethanol solution for 16 h at 25 °C to form a mixed MUA/MPA self-assembly layer. Then, MPA was stripped off from the Au electrode by linear scanning from −0.1 to −1.0 V in 0.5 M NaOH solution to obtain the porous MUA layer (Figure S2 in the Supporting Information). After being thoroughly rinsed with ethanol and deionized water, 0.15 mL of DOPC vesicle solution was added on the porous MUA layer under pH 8.5 for 2 h to form a BLM coating. Finally, the electrode was immersed into 4 mM MUA ethanol solution at 25 °C for 1 h to block the unmodified region of the gold surface. Each step in the above fabrication process was characterized by CV and EIS to obtain reproducible results (Figure S3 in the Supporting Information). The BLM-based sensor should be prepared and used for the oligomer determinations on the same day.

Preparation of Aβ_{40} and Aβ_{42} Monomers and Oligomers. Lyophilized Aβ_{40} and Aβ_{42} peptides were dissolved in HFIP at a final concentration of 1 mg·mL^{-1} at 4 °C for 2 h. After being sonicated for 30 min, the solution was centrifuged at 14,000 rpm for 30 min at 4 °C in an Eppendorf 5417R centrifuge (Eppendorf, Hamburg, Germany) to remove any existing aggregates. The supernatant was lyophilized at −100 °C on a freeze dryer (LaboGene ScanVac CoolSafe 110-4 Pro freeze dryer, Denmark) to obtain a purified Aβ_{40} and

https://dx.doi.org/10.1021/acs.analchem.0c05281
Anal. Chem. 2021, 93, 3611−3617

$A\beta_{42}$ monomer ($A\beta_{40}M$ and $A\beta_{42}M$). The $A\beta_{40}M$ and $A\beta_{42}M$ solutions were then prepared by dissolving the obtained lyophilized powder in PBS (10 mM, pH 7.4, 0.1 M NaCl) at a desired concentration. The concentrations of $A\beta_{40}M$ and $A\beta_{42}M$ solutions were calculated from the UV−vis spectra at 276 nm by setting the extinction coefficient ε of 1410 $M^{-1}\cdot cm^{-1}$ for tyrosine.

L-$A\beta_{40}O$ was prepared following our previous work.[25] Briefly, 100 μM $A\beta_{40}M$ solution was incubated at 37 °C for 12 h. Then, the solution was filtrated through a 10 kDa cutoff Millipore (YM-10) membrane (Millipore, Billerica, MA) and used as the L-$A\beta_{40}O$ solution. L-$A\beta_{42}O$ was prepared by incubating 50 μM $A\beta_{42}M$ at 37 °C for 5 h and filtrating it through the Millipore YM-10 membrane. The apparent concentrations of obtained L-$A\beta_{40}O$ and L-$A\beta_{42}O$ were respectively calculated as equivalent to the corresponding monomer concentrations, determined from the absorption at 276 nm.

Preparation of the Human CSF Samples. The CSF samples from healthy donors were provided by the Third Xiangya Hospital of Central South University. All of the protocols were reviewed by the Joint Ethics Committee of the Central South University Health Authority and performed in accordance with national guidelines. The CSF samples were collected by lumbar puncture using a 22 gauge quincke-type needle, aliquoted, and stored at −80 °C for later use. Before each measurement, the CSF samples were filtrated through the Millipore YM-10 membrane to reduce the disturbances from coexisting larger $A\beta$ oligomers/fibrils and other proteins. Then, 1 mM EDTA and 1 mM ascorbic acid were added into the CSF solution to reduce the disturbances from metal ions such as Cu^{2+} and coexisting oxidized species such as lipid peroxide.

RESULTS AND DISCUSSION

Design Strategy of this Electrochemical Sensor. Figure 1A illustrates the preparation of the BLM-based electrochemical sensor and the determination of two oligomers. Briefly, a porous MUA layer is prepared on the Au electrode via selective electrochemical desorption of MPA from a mixed MUA/MPA self-assembly monolayer (SAM), according to our previous work.[24] Subsequently, the BLM-based electrochemical sensor is fabricated by spreading DOPC vesicles on the porous MUA layer and blocking those uncovered inner pores in the MUA layer with free MUA molecules. In the determination process, the electrochemical sensor is incubated with the mixture of two oligomers and a redox probe $[Fe(CN)_6]^{3-/4-}$. The oligomer-induced membrane damage is characterized by EIS and quantified by fitting the EIS curve with an equivalent electric circuit (EEC) in Figure 1B. The value of $R_{ct\text{-}in}$ in the EEC, representing the charge-transfer resistance of the metal/inner pore interface, is highly sensitive to the changes on membrane damage. Then, according to the different membrane damage dynamics of two oligomers, the EIS responses are measured at two critical points of time corresponding to the membrane damage entirely by L-$A\beta_{42}O$ and by the mixture of two oligomers. The obtained values of $R_{ct\text{-}in}$ are used to quantify L-$A\beta_{42}O$ and L-$A\beta_{40}O$.

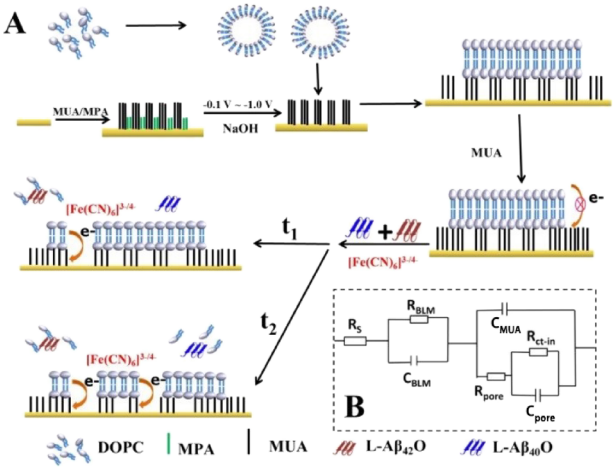

Figure 1. (A) Schematic illustration of the EIS detections of L-$A\beta_{42}O$ and L-$A\beta_{40}O$. (B) Equivalent circuits used to simulate the impedance data.

This BLM-based electrochemical sensor is anticipated to possess the following distinguishing features. First, according to the dynamic differences on membrane damage induced by L-$A\beta_{42}O$ and L-$A\beta_{40}O$, the sensor achieves the determinations of both $A\beta$ oligomers in one chip. The method is label-free, antibody-free, highly selective, and has a relatively low cost, and no specific recognition element or amplification strategy is needed. Also, it is the first report on simultaneous detections of L-$A\beta_{42}O$ and L-$A\beta_{40}O$ by a sensor. Second, the ultralow aspect ratio of the inner pore in the MUA layer is favorable for the mass transfer of $[Fe(CN)_6]^{3-/4-}$ onto the electrode surface once the BLM is damaged. It will cause significant changes in interface characteristics and improve detection sensitivity. Third, the usage of weakly charged DOPC (isoelectric point: 6.7) decreases non-specific adsorption of coexisting proteins in CSF, ensuring the applicability of the sensor.

Concentration Calibration of the Prepared L-$A\beta_{42}O$ and L-$A\beta_{40}O$ Solutions. In this work, L-$A\beta_{42}O$ and L-$A\beta_{40}O$ were prepared by incubating the corresponding monomer solutions for 5 and 12 h, respectively. After removing those coexisting big aggregates by ultrafiltration, the apparent concentrations of both oligomer solutions, defined as the equivalent concentration to that of the monomer, were calculated by the UV−vis spectra at 276 nm by setting the extinction coefficient ε of 1410 $M^{-1}\cdot cm^{-1}$ for tyrosine. However, according to the reaction equilibrium between monomers and aggregates, both oligomer solutions must be mixtures of oligomers and corresponding monomers. To quantify the composition of the obtained L-$A\beta_{42}O$ and L-$A\beta_{40}O$ solution, SEC measurements were performed. As shown in Figure 2, the dimer and monomer are the main

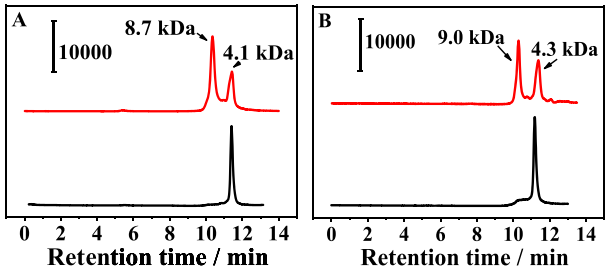

Figure 2. Size-exclusion chromatograms of L-$A\beta_{40}O$ (A) and L-$A\beta_{42}O$ (B) solutions (red line) at an apparent concentration of 10 μM. The black lines in both panels correspond to 10 μM $A\beta_{40}M$ and 10 μM $A\beta_{42}M$.

https://dx.doi.org/10.1021/acs.analchem.0c05281
Anal. Chem. 2021, 93, 3611−3617

forms in both oligomer solutions. By integrating the peak areas, the molar ratios of L-Aβ_{42}O/Aβ_{42}M and L-Aβ_{40}O/Aβ_{40}M were obtained to be 1.10 ± 0.16 and 1.55 ± 0.19, respectively. It means that, at the same apparent concentration of 10 μM, the exact concentrations of L-Aβ_{42}O and L-Aβ_{40}O, expressed as equivalent to the corresponding monomer concentrations, are 5.23 and 6.08 μM, respectively. Based on it, all the concentrations of prepared L-Aβ_{40}O and L-Aβ_{42}O were calibrated in this work. Note that, although only monomers and dimers were detected by SEC, the coexistence of other low-mass, soluble oligomers (i.e., trimers and pentamers) in ultralow concentrations was highly probable.[26] Therefore, we defined the obtained solutions as L-Aβ_{40}O and L-Aβ_{42}O, not as dimer solutions.

Feasibility of the BLM-Based Electrochemical Sensor for L-Aβ_{42}O and L-Aβ_{40}O Detections. The detection feasibility of the BLM-based electrochemical sensor depends on two factors, the usage of an appropriate parameter for the evaluation of membrane damage and the distinct dynamic differences on membrane damage induced by L-Aβ_{42}O and L-Aβ_{40}O. In this work, to extract the electrical properties in the membrane damage process, an EEC commonly used for an electrode coated with two inert porous layers[27] was adopted to fit the EIS responses. The EEC as depicted in Figure 1 includes the parallel combination of $R_{ct\text{-}in}$ (charge-transfer resistance) and C_{pore} (double-layer capacitance) corresponding to the impedance at the inner pore/metal interface. R_{pore} is the electrolyte resistance within the inner pore length. The insulating part of the porous MUA layer is considered as a capacitor C_{MUA}, which is in parallel with the impedance in the inner pore. The effect of the outer BLM layer is taken into account with an additional series $R_{BLM}C_{BLM}$ circuit. R_s is the resistance of the electrolyte solution. Using the EEC, those impedance responses from oligomer- or monomer-treated BLM-based sensors were fitted.

Here, both Nyquist and Bode plots are displayed because they can provide more details (Figure 3). Obviously, the fitting curves show good agreement with experimental data, demonstrating that the EEC is appropriate for describing the EIS behaviors of the system.

In Figure 3, oligomer-treated sensors display significant changes on EIS responses, which are quite different from monomer-treated sensors, confirming the oligomer-induced membrane damage.[24] Based on it, Table 1 lists two membrane-related resistance parameters extracted from the fitting results of oligomer-treated sensors. All R_{BLM} values are above 1 MΩ, in accordance with the reported value of the BLM.[28] The value of $R_{ct\text{-}in}$ is at the MΩ level, indicating that most of the porous MUA surfaces are blocked by the BLM. As expected, both R_{BLM} and $R_{ct\text{-}in}$ display significant oligomer-related changes. However, due to the mediocre reproducibility on the sensor fabrication, both parameters display large deviations in three replicated experiments. To reduce the systematic errors, we normalized the values with the corresponding value at 0 h. As shown in Table 1, normalized $R_{ct\text{-}in}$ values display small standard deviations, while normalized R_{BLM} values maintain large standard deviations. The large standard deviations on R_{BLM} should be attributed to the non-specific adsorption of stripped phospholipids or phospholipid/oligomer complexes on the BLM or MUA layer. Therefore, to ensure the reproducibility of the detection, we choose normalized $R_{ct\text{-}in}$ (defined as R') to quantify the oligomer-induced membrane damage.

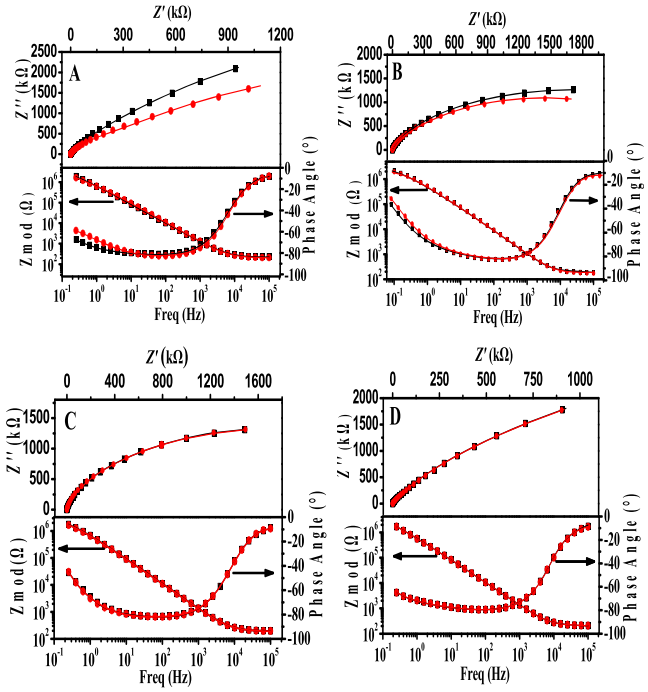

Figure 3. EIS in Nyquist (top panel) and Bode (bottom panel) plots of the BLM-based sensor in 5 mM $[Fe(CN)_6]^{3-/4-}$ solution at zero bias after being incubated with 1 μM L-Aβ_{42}O (A), L-Aβ_{40}O (B), Aβ_{42}M (C), and Aβ_{40}M (D) for 0 (black symbols) or 2 h (red symbols), respectively. Solid lines in each panel are fittings using the EEC.

Table 1. Membrane-Related Resistance Parameters for the BLM-Based Sensor Incubated with Aβ Oligomers

		R_{BLM} (MΩ)	$R_{ct\text{-}in}$ (MΩ)
L-Aβ_{42}O	sample 1/blank 1	1.85/1.05	3.18/7.55
	normalized	1.76	0.42
	sample 2/blank 2	2.60/1.00	3.23/6.88
	normalized	2.60	0.47
	sample 3/blank 3	2.20/1.10	3.38/7.00
	normalized	2.00	0.48
	standard deviation	43.3%	3.2%
L-Aβ_{40}O	sample 1/blank 1	2.08/1.24	4.53/7.72
	normalized	1.68	0.58
	sample 2/blank 2	2.53/1.09	5.13/8.30
	normalized	2.32	0.62
	sample 3/blank 3	1.76/1.12	4.02/6.42
	normalized	1.57	0.63
	standard deviation	40.5%	2.6%

The second factor on the detection feasibility is whether L-Aβ_{42}O and L-Aβ_{40}O display significant difference on membrane damage dynamics. Here, we investigated the time-dependent membrane damage induced by Aβ oligomers and monomers. As shown in Figure 4, both Aβ monomers induce no detectable changes of the R' values within 2.5 h, which is in accordance with the fact that Aβ monomers at low concentrations cannot induce rapid hole formation in the lipid membrane.[29,30] Meanwhile, both Aβ oligomers induce significant R' changes while the time-dependent curves display quite different features. L-Aβ_{42}O induces the decrease of R' once it is introduced onto the sensor, corresponding to a quick damage on the membrane.[31] The value of R' attenuates to a

https://dx.doi.org/10.1021/acs.analchem.0c05281
Anal. Chem. 2021, 93, 3611−3617

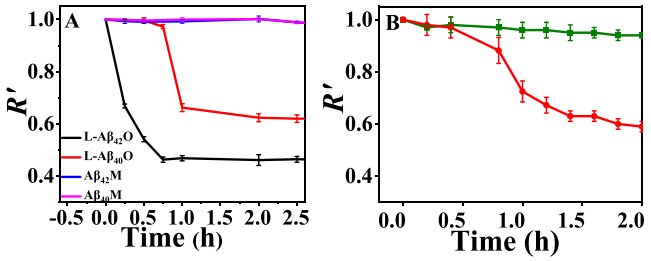

Figure 4. (A) Time dependence of R' from the BLM-based sensor incubated with 1 μM Aβ oligomers or monomers. (B) Time dependence of R' from the BLM-based sensor (red symbols) or a BLM-covered compact MUA SAM (green symbols) incubated with 1 μM Aβ_{40}.

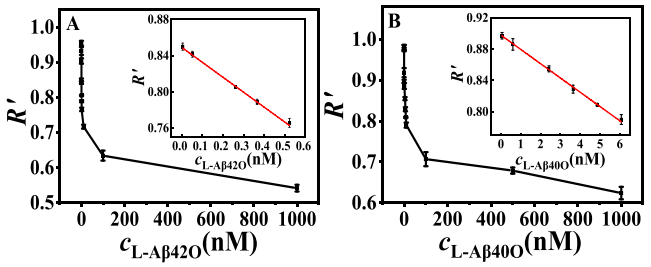

Figure 5. Relationship between R' and the concentration of L-Aβ_{42}O (A) and L-Aβ_{40}O (B). Inserted is the linear relationship between R' and $c_{\text{L-A}\beta\text{42O}}$ (A) and $c_{\text{L-A}\beta\text{40O}}$ (B).

plateau when the incubation time is approximately 45 min. Comparatively, L-Aβ_{40}O induces a much slow damage process. The detectable decrease of R' appears when the incubation time is over 30 min and reaches a plateau at ∼2 h. The significant dynamic differences should be attributed to the structural differences between two oligomers. Compared to Aβ_{40}, Aβ_{42} has two more hydrophobic amino acids at the C-terminal, which belong to the transmembrane part of amyloid-β precursor protein. Therefore, L-Aβ_{42}O usually directly incorporates into planar bilayers and induces membrane damage following the first-order kinetics,[32−35] while L-Aβ_{40}O has to transfer into pentamers or octamers before it induces observed membrane damage.[36−38] Our data display obvious first-order kinetics on L-Aβ_{42}O-induced membrane damage with an equation of $R' = 0.41 + 0.57e^{-2.36t}$ and a two-step autocatalytical growth kinetics on L-Aβ_{40}O-induced membrane damage with an equation of $R' = 0.62 + 19.95/(49.43 + 3.08e^{19.95t})$ (Figure S4 in the Supporting Information). Based on it, the half-life time for the L-Aβ_{42}O/BLM interaction (∼20 min), which is independent of the initial concentration of L-Aβ_{42}O and at which the response from L-Aβ_{40}O is undetectable, is chosen as the incubation time for the detection of L-Aβ_{42}O. Meanwhile, an incubation time of 60 min is chosen as the incubation time for the detection of L-Aβ_{40}O to achieve a time-saving effect.

The effect of the porous structure on the membrane damage measurement was also verified. As shown in Figure 4B, L-Aβ_{40}O induces much more significant EIS response changes on the porous MUA-supported BLM than those on the compact MUA SAM-supported BLM. It is exactly what we anticipated. According to our previous research, in the porous MUA layer, the size of these inner pores ranges from 12 to 19 nm while the inner pore height is no more than 2 nm.[24] The ultralow aspect ratio of the inner pores facilitates the influx of $[Fe(CN)_6]^{3-/4-}$ from the solution bulk to the electrode surface. On the contrary, in the compact MUA SAM-supported BLM, due to the lack of porous structure, the probe influx onto the electrode is hindered. Although some pinholes may exist on the compact MUA SAM, their small size and high hydrophobicity are still disadvantageous to the influx. Therefore, the porous structure is necessary for providing significant changes of interface characteristics and improving detection sensitivity.

Sensitivity and Selectivity of this Electrochemical Sensor. Figure 5 displays the EIS responses of the sensor after treatment with L-Aβ_{42}O or L-Aβ_{40}O under different concentrations. As shown in the insets, the method displays high sensitivity for determinations of both Aβ oligomers. A good linear relationship between R' and $c_{\text{L-A}\beta\text{42O}}$ ranges from 5 to 500 pM, with a detection limit of 3 pM. The linear equation is $R' = -0.166c_{\text{L-A}\beta\text{42O}} + 0.847$ ($R^2 = 0.998$). The linear detection range for L-Aβ_{40}O is from 60 pM to 6 nM, with a detection limit of 26 pM. The linear equation is $R' = -0.0182c_{\text{L-A}\beta\text{40O}} + 0.898$ ($R^2 = 0.999$).

In the context of what is known from reported in vitro and in vivo experiments,[39] interferences that may coexist with Aβ oligomers in CSF include Aβ_{42}M and Aβ_{40}M, insulin (∼5.8 kDa), tau protein (∼45 kDa), α-synuclein (∼19 kDa), a serum amyloid P component (∼25 kDa), transthyretin (∼55 kDa), etc. After being treated with a 10 kDa cutoff membrane, those proteins with a molecular weight over 30 kDa were completely removed. Based on it, only low-mass peptides including insulin, Aβ_{42}M, and Aβ_{40}M were chosen to evaluate the selectivity of this method. As shown in Figure 6A, in the detection of L-Aβ_{42}O, these interfering species with 200 times higher concentrations result in no significant changes on EIS responses. Similarly, in the detection of L-Aβ_{40}O, these interfering species with 200 times higher concentrations result in no significant changes on EIS responses (Figure 6B). It confirms the excellent selectivity of our method toward corresponding biomarkers.

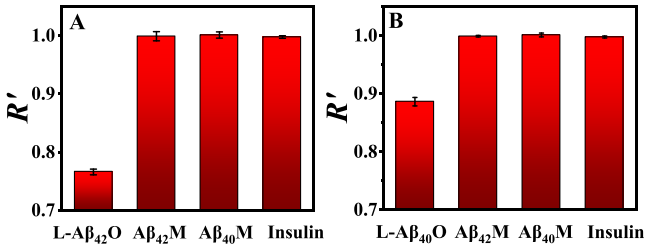

Figure 6. EIS responses of the BLM-based sensor to 500 pM L-Aβ_{42}O, 500 pM L-Aβ_{40}O, 100 nM Aβ_{42}M, 100 nM Aβ_{40}M, and 100 nM insulin. The detection times were 20 (A) and 60 min (B).

Applicability of this Electrochemical Sensor. The applicability of this method was assessed in ACSF and human CSF spiked with L-Aβ_{42}O and L-Aβ_{40}O, respectively. The recoveries in ACSF samples range from 95.7 to 102.6% for L-Aβ_{42}O and from 94.4 to 105.0% for L-Aβ_{40}O (Table 2). The ACSF solutions spiked with mixed L-Aβ_{42}O and L-Aβ_{40}O were also determined. Note that, in the mixed oligomer samples, L-Aβ_{42}O was quantified directly according to the measured response and corresponding linear equation. However, for the determination of L-Aβ_{40}O, the response of L-Aβ_{42}O (double the R' value at 20 min) must be deducted from the R' value at 60 min, and then, quantitative analysis was made according to the calibration curve. As a result, in Table 3, all the recoveries of L-Aβ_{40}O are inferior to those of L-Aβ_{42}O. Meanwhile, the

https://dx.doi.org/10.1021/acs.analchem.0c05281
Anal. Chem. 2021, 93, 3611−3617

Table 2. Recoveries of Independent L-Aβ_{42}O and L-Aβ_{40}O in ACSF Samples

	sample	added (nM)	found (nM)	recovery (%)
L-Aβ_{42}O	1	0		
	2	0.026	0.025 ± 0.002	98.1 ± 8.0
	3	0.200	0.191 ± 0.008	95.7 ± 4.0
	4	0.420	0.431 ± 0.007	102.6 ± 1.6
L-Aβ_{40}O	5	0		
	6	0.300	0.283 ± 0.012	94.4 ± 4.0
	7	2.430	2.471 ± 0.122	101.7 ± 5.1
	8	4.860	5.104 ± 0.426	105.0 ± 8.8

Table 3. Recoveries of Mixed L-Aβ_{42}O and L-Aβ_{40}O in ACSF Samples

	sample	added (nM)	found (nM)	recovery (%)
L-Aβ_{42}O	1	0		
	2	0.200	0.204 ± 0.018	102.0 ± 8.4
	3	0.420	0.444 ± 0.024	105.7 ± 5.6
L-Aβ_{40}O	1	0		
	2	2.430	2.473 ± 0.330	101.8 ± 13.3
	3	4.860	4.500 ± 0.501	92.6 ± 11.1

recoveries in mixed L-Aβ_{42}O and L-Aβ_{40}O are slightly inferior to those in independent samples, indicating some uncertain disturbances between L-Aβ_{42}O and L-Aβ_{40}O. Even so, the good stability and reproducibility shown in Table 3 are enough for its further application in real sample detections. Finally, the BLM-based electrochemical biosensor was employed to measure L-Aβ_{42}O or L-Aβ_{40}O in undiluted and 10-fold diluted human CSF samples from health donors, but no detectable $R_{ct\text{-}in}$ changes appeared. The results indicate that the concentrations of both oligomers in a healthy person's CSF are at the pM level or even lower, which is in accordance with those reported data.[25,40,41] Additionally, the results confirm that those coexisting substances in CSF have no detectable interferences on the oligomer detection. One thing that should be emphasized is that the CSF samples must be pretreated with EDTA and ascorbic acid. Otherwise, the coexisting metal ions and other oxides will induce serious membrane damage (Figure S5 in the Supporting Information). The diluted CSF samples spiked with L-Aβ_{42}O or L-Aβ_{40}O at different concentrations were also investigated. All recoveries listed in Table 4 confirm that the BLM-based electrochemical biosensor

Table 4. Recoveries of Mixed L-Aβ_{42}O and L-Aβ_{40}O in Human CSF Samples

	sample	added (nM)	found (nM)	recovery (%)
L-Aβ_{42}O	1	0		
	2	0.200	0.210 ± 0.017	104.8 ± 8.1
	3	0.420	0.385 ± 0.012	91.6 ± 3.1
L-Aβ_{40}O	1	0		
	2	2.430	2.543 ± 0.318	108.8 ± 12.5
	3	4.860	4.558 ± 0.317	93.8 ± 7.0

can achieve good performance for both L-Aβ_{42}O and L-Aβ_{40}O determinations in the CSF samples. One thing that should be mentioned is that, due to the lack of CSF samples from AD patients, we cannot provide the exact concentration distribution of both oligomers in AD patients in this work. However, according to the linear range of the sensor and its recoveries in CSF samples, we are confident in its application in clinic.

CONCLUSIONS

In this study, according to the dynamic differences on the membrane damages induced by two oligomers, a BLM-based electrochemical biosensor was developed for the determinations of both L-Aβ_{42}O and L-Aβ_{40}O by electrochemical impedance spectroscopy. Using this electrochemical biosensor, L-Aβ_{42}O was determined within 20 min, with a linear range from 5 to 500 pM and a detection limit of 3 pM. Meanwhile, L-Aβ_{40}O was determined within 60 min, with a linear range from 60 pM to 6.0 nM and a detection limit of 26 pM. Although the recoveries in mixed L-Aβ_{42}O and L-Aβ_{40}O are slightly inferior to those in independent samples, the good recoveries of this proposed method in ASCF and CSF samples are enough for its further application in real sample detections. This work provides an antibody-free, time-saving, highly selective, and sensitive method. More importantly, for the first time, this work provides a one-element sensor strategy for simultaneous determinations of L-Aβ_{42}O and L-Aβ_{40}O, and no other recognition element or amplification strategy is needed. Although the present stability and reproducibility of this method are not excellent, there are still many ways to improve this problem in a future work. This includes, but is not limited to, optimizing the membrane composition to improve the stability of the membrane on the solution/supporting material interface, modifying new functional groups on the membrane to improve its specific susceptibility to different oligomers so as to improve the accuracy and reproducibility, and extending the applications of this method to more different oligomers.

ASSOCIATED CONTENT

Supporting Information

The Supporting Information is available free of charge at https://pubs.acs.org/doi/10.1021/acs.analchem.0c05281.

Figures showing a fluorescent image and dynamic light scattering of DOPC vesicles (Figure S1); linear sweep voltammograms of MPA, MUA, or mixed MPA/MUA SAM for fabrication of porous MUA SAM (Figure S2); CV and EIS in the Nyquist plot corresponding to the successive fabrication of the BLM-based electrochemical sensor (Figure S3); kinetic fitting results of two oligomer-induced membrane damages (Figure S4); and EIS in Nyquist plots of the BLM-based electrochemical sensor after being incubated with CSF pretreated with or without EDTA/ascorbic acid (Figure S5) (PDF)

AUTHOR INFORMATION

Corresponding Author

Juan Xiang − *Hunan Provincial Key Laboratory of Micro & Nano Materials Interface Science, College of Chemistry and Chemical Engineering, Central South University, Changsha 410083, P. R. China;* orcid.org/0000-0001-7320-8441; Phone: +86-731-88876490; Email: xiangj@csu.edu.cn; Fax: +86-731-88879616

Authors

Yuemei Duan − *Hunan Provincial Key Laboratory of Micro & Nano Materials Interface Science, College of Chemistry and Chemical Engineering, Central South University, Changsha 410083, P. R. China*

Jia Chen − *Hunan Provincial Key Laboratory of Micro & Nano Materials Interface Science, College of Chemistry and*

https://dx.doi.org/10.1021/acs.analchem.0c05281
Anal. Chem. 2021, 93, 3611−3617

Chemical Engineering, Central South University, Changsha 410083, P. R. China

Yan Jin − *Operation Center, The Third Xiangya Hospital, Central South University, Changsha 410013, China*

Qiuyun Tu − *Department of Geriatrics, The Fifth Affiliated Hospital of Sun Yat-Sen University, Zhuhai 519000, China*

Shuhui Wang − *Hunan Provincial Key Laboratory of Micro & Nano Materials Interface Science, College of Chemistry and Chemical Engineering, Central South University, Changsha 410083, P. R. China*

Complete contact information is available at: https://pubs.acs.org/10.1021/acs.analchem.0c05281

Author Contributions

‡Y.D. and J.C. contributed equally to the work. The manuscript was written through contributions of all authors. All authors have given approval to the final version of the manuscript.

Notes

The authors declare no competing financial interest.

■ ACKNOWLEDGMENTS

This work was financially supported by the National Natural Science Foundation of China (21573290), the Open Research Fund of State Key Laboratory of Physical Chemistry of Solid Surface, Xiamen (201814), the State Key Laboratory of Fine Chemicals, Dalian University of Technology (KF1910), and the Hunan Provincial Science and Technology Plan Project, China (no. 2019TP1001).

■ REFERENCES

(1) DeTure, M. A.; Dickson, D. W. *Mol. Neurodegener.* **2019**, *14*, 32−50.
(2) Li, S.; Selkoe, D. J. *J. Neurochem.* **2020**, *154*, 583−597.
(3) Selkoe, D. J.; Hardy, J. *EMBO Mol. Med.* **2016**, *8*, 595−608.
(4) Sunde, M.; Serpell, L. C.; Bartlam, M.; Fraser, P. E.; Pepys, M. B.; Blake, C. C. F. *J. Mol. Biol.* **1997**, *273*, 729−739.
(5) Fezoui, Y.; Hartley, D. M.; Harper, J. D.; Khurana, R.; Walsh, D. M.; Condron, M. M.; Selkoe, D. J.; Lansbury, P. T.; Fink, A. L.; Teplow, D. B. *Amyloid* **2000**, *7*, 166−178.
(6) Lee, S. J. C.; Nam, E.; Lee, H. J.; Savelieff, M. G.; Lim, M. H. *Chem. Soc. Rev.* **2017**, *46*, 310−323.
(7) Bitan, G.; Kirkitadze, M. D.; Lomakin, A.; Vollers, S. S.; Benedek, G. B.; Teplow, D. B. *Proc. Natl. Acad. Sci. U. S. A.* **2002**, *100*, 330−335.
(8) Shoji, M.; Kanai, M. *J. Alzheimer's Dis.* **2001**, *3*, 313−321.
(9) Bruggink, K. A.; Jongbloed, W.; Biemans, E. A. L. M.; Veerhuis, R.; Claassen, J. A. H. R.; Kuiperij, H. B.; Verbeek, M. M. *Anal. Biochem.* **2013**, *433*, 112−120.
(10) Rama, E. C.; González-García, M. B.; Costa-García, A. *Sens. Actuators, B* **2014**, *201*, 567−571.
(11) Teoh, C. L.; Su, D.; Sahu, S.; Yun, S.-W.; Drummond, E.; Prelli, F.; Lim, S.; Cho, S.; Ham, S.; Wisniewski, T.; Chang, Y.-T. *J. Am. Chem. Soc.* **2015**, *137*, 13503−13509.
(12) Ke, H.; Sha, H.; Wang, Y.; Guo, W.; Zhang, X.; Wang, Z.; Huang, C.; Jia, N. *Biosens. Bioelectron.* **2018**, *100*, 266−273.
(13) Kayed, R.; Glabe, C. G. *Methods Enzymol.* **2006**, *413*, 326−344.
(14) Tsukakoshi, K.; Abe, K.; Sode, K.; Ikebukuro, K. *Anal. Chem.* **2012**, *84*, 5542−5547.
(15) Xia, N.; Wang, X.; Yu, J.; Wu, Y.; Cheng, S.; Xing, Y.; Liu, L. *Sens. Actuators, B* **2017**, *239*, 834−840.
(16) Hillen, H.; Barghorn, S.; Striebinger, A.; Labkovsky, B.; Muller, R.; Nimmrich, V.; Nolte, M. W.; Perez-Cruz, C.; van der Auwera, I.; van Leuven, F.; van Gaalen, M.; Bespalov, A. Y.; Schoemaker, H.; Sullivan, J. P.; Ebert, U. *J. Neurosci.* **2010**, *30*, 10369−10379.
(17) Zhang, Y.; Figueroa-Miranda, G.; Lyu, Z.; Zafiu, C.; Willbold, D.; Offenhäusser, A.; Mayer, D. *Sens. Actuators, B* **2019**, *288*, 535−542.
(18) Hu, Y.; Su, B.; Zheng, H.; Kim, J. R. *Mol. BioSyst.* **2012**, *8*, 2741−2752.
(19) Jiang, M.; Wang, X.-Y.; Wang, X.-B. *Chin. J. Anal. Chem.* **2018**, *46*, 1339−1349.
(20) Zheng, W.; Tsai, M.-Y.; Wolynes, P. G. *J. Am. Chem. Soc.* **2017**, *139*, 16666−16676.
(21) Nguyen, P. H.; Campanera, J. M.; Ngo, S. T.; Loquet, A.; Derreumaux, P. *J. Phys. Chem. B* **2019**, *123*, 3643−3648.
(22) Phillips, J. C. *ACS Chem. Neurosci.* **2019**, *10*, 2843−2847.
(23) Yamaguchi, T.; Nomura, M.; Matsuoka, T.; Koda, S. *Chem. Phys. Lipids* **2009**, *160*, 58−62.
(24) Zhang, M.; Zhai, Q.; Wan, L.; Chen, L.; Peng, Y.; Deng, C.; Xiang, J.; Yan, J. *Anal. Chem.* **2018**, *90*, 7422−7427.
(25) Deng, C.; Liu, H.; Zhang, M.; Deng, H.; Lei, C.; Shen, L.; Jiao, B.; Tu, Q.; Jin, Y.; Xiang, L.; Deng, W.; Xie, Y.; Xiang, J. *Anal. Chem.* **2018**, *90*, 1710−1717.
(26) Jan, A.; Hartley, D. M.; Lashuel, H. A. *Nat. Protoc.* **2010**, *5*, 1186−1209.
(27) Orazem, M. E.; Tribollet, B. *Electrochim. Acta* **2008**, *53*, 7360−7366.
(28) Ragheb, T.; Riegle, S.; Geddes, L. A.; Amin, V. *Ann. Biomed. Eng.* **1992**, *20*, 617−627.
(29) Morinaga, A.; Hasegawa, K.; Nomura, R.; Ookoshi, T.; Ozawa, D.; Goto, Y.; Yamada, M.; Naiki, H. *Biochim. Biophys. Acta* **2010**, *1804*, 986−995.
(30) Kotarek, J. A.; Moss, M. A. *Anal. Biochem.* **2010**, *399*, 30−38.
(31) Relini, A.; Marano, N.; Gliozzi, A. *Adv. Colloid Interface Sci.* **2014**, *207*, 81−92.
(32) Henry, S.; Vignaud, H.; Bobo, C.; Decossas, M.; Lambert, O.; Harte, E.; Alves, I. D.; Cullin, C.; Lecomte, S. *Biomacromolecules* **2015**, *16*, 944−950.
(33) Phan, H. T. T.; Shimokawa, N.; Sharma, N.; Takagi, M.; Vestergaard, M. C. *Biochem. Biophys. Rep.* **2018**, *14*, 98−103.
(34) Demuro, A.; Smith, M.; Parker, I. *J. Cell Biol.* **2011**, *195*, 515−524.
(35) Williams, T. L.; Serpell, L. C. *FEBS J.* **2011**, *278*, 3905−3917.
(36) Johnson, R. D.; Steel, D. G.; Gafni, A. *Protein Sci.* **2014**, *23*, 869−883.
(37) Schauerte, J. A.; Wong, P. T.; Wisser, K. C.; Ding, H.; Steel, D. G.; Gafni, A. *Biochemistry* **2010**, *49*, 3031−3039.
(38) Williams, T. L.; Day, I. J.; Serpell, L. C. *Langmuir* **2010**, *26*, 17260−17268.
(39) Luo, J.; Wärmländer, S. K. T. S.; Gräslund, A.; Abrahams, J. P. *J. Biol. Chem.* **2016**, *291*, 16485−16493.
(40) Zhao, Y.; Li, X.; Yang, Y.; Si, S.; Deng, C.; Wu, H. *Biosens. Bioelectron.* **2020**, *149*, 111840.
(41) Savage, M. J.; Kalinina, J.; Wolfe, A.; Tugusheva, K.; Korn, R.; Cash-Mason, T.; Maxwell, J. W.; Hatcher, N. G.; Haugabook, S. J.; Wu, G.; Howell, B. J.; Renger, J. J.; Shughrue, P. J.; McCampbell, A. *J. Neurosci.* **2014**, *34*, 2884−2897.